PCCP

Accepted Manuscript

Journal Name

ARTICLE

Green Apatite: Hydride Ion, Electron and Their Interconversion in the Crystallographic Channel

Received 00th January 20xx,
Accepted 00th January 20xx

DOI: 10.1039/x0xx00000x

www.rsc.org/

Katsuro Hayashi*[a] and Hideo Hosono[b]

Hydride (H^-) ions and electrons in channel sites of the lattice of calcium phosphate apatite are characterized. Solid-state chemical reduction using TiH_2 is effective for doping of H^- ions into apatite. Irradiation of the H^- ion-doped apatite with ultraviolet (UV) light induces green coloration. Electron paramagnetic resonance (EPR) reveals that this colour centre is attributed to electrons captured at a vacant anion site in the crystallographic channel, forming F^+ centres. Transient H^0 atoms are detected at low temperatures by EPR. The concentration of UV-induced electrons in the apatite at room temperature decays according to second-order kinetics because of chemical reactions involving two electrons; overall, electron generation and thermal decay can be described as: $H^- + O^{2-} \leftrightarrow 2e^- + OH^-$. ^1H magic angle spinning nuclear magnetic resonance spectroscopy is used to identify H^- ions in the apatite, which are characterized by a chemical shift of +3.4 ppm. Various types of O-H groups including OH^- ions in the channel and protons bound to phosphate groups are concurrently formed, and are identified by considering the relationship between O-H stretching frequency and ^1H chemical shift. Complementary results obtained by EPR and NMR reveal that the H^- ions and transient H^0 atoms are located at the centre of Ca_3 triangles in apatite, while the electrons are located in the centre of Ca_6 octahedra. These findings provides an effective approach for identifying new classes of mixed-oxide- hydride or -electride crystals.

1. Introduction

Apatites are a complex and diverse class of materials.[1] Among this large family of isomorphs, hydroxyapatite (HAp), which is a crystallographical analogue of calcified tissues of vertebrates, is becoming increasingly important as a biomaterial. Many synthetic bone substitutes consisting of HAp are now commercially available to repair lost or damaged tissues.[2,3] Apatites are also well known for their surface-binding and cation-exchange properties towards various organic and inorganic substances,[4,5] and their applications are expanding to catalysts,[6] chromatographic columns[7] and fluorescence host materials.[8]

Calcium phosphate apatites generally crystallize in a hexagonal system (space group $P6_3/m$) and are characterized by an isolated tetrahedron of PO_4^{3-} and two Ca^{2+}-ion sites. The Ca2 site, forms an array of triangles running along the *c*-axis. The inside of these triangles is often referred to as a 'channel', and is partially or completely occupied by various kinds of anions. The general formula of the unit cell of calcium phosphate apatite is described as,

$$[Ca_{10}(PO_4)_6]^{2+}\cdot X^{2-}, \qquad (1)$$

where the brackets are used to emphasize the positively charged host lattice that incorporates guest anions ($X^{2-} = 2F^-$, $2Cl^-$, $2Br^-$, $2OH^-$, CO_3^{2-}, O^{2-}) as the counter ions. The channel sites are usually occupied by an admixture of these anions. Assuming a defect-free lattice, the total concentration of anions is equivalent to 3.8×10^{21} e cm^{-3}. However, the host lattice generally contains defects such as Ca deficiency [9,10] and acidic protons that form HPO_4^{2-} groups.[9] The occupied sites in the channel depend on the guest anion. F^- and O^{2-} ions [11,12] are found at the centre of Ca_3 triangles, while OH^- and Cl^- ions are observed at an off-triangle plane along the *c*-axis. Under certain conditions, the off-centre anions are ordered, which is accompanied with a slight distortion in the lattice that leads to a change in crystal symmetry to $P2_1/b$.[13] Incorporation of CO_3^{2-} ions and/or dehydroxylation ($2OH^- \rightarrow O^{2-}$) at high temperatures promote crystallographic transition between some hexagonal and monoclinic forms of calcium phosphate apatite.[14] Nevertheless, approximation of the host lattice as hexagonal symmetry may be convenient for understanding essential properties of apatites. The channel sites are also partially occupied by diatomic oxygen ions O_2^{2-} [15] and O_2^{-}.[16] Formation of O^- [17–19] and $^\bullet OH$ [20] species has also been found in radiation-irradiated apatites. Electron paramagnetic resonance (EPR) has played a central role in characterization of paramagnetic species in apatites.

---

[a] Department of Applied Chemistry, Kyushu University, West-3, Motooka 744, Fukuoka 891-0395, Japan. E-mail: k.hayashi@cstf.kyushu-u.ac.jp

[b] Frontier Research Centre, Tokyo Institute of Technology, and ACCEL Project, Japan Science and Technology Agency, S2-13, 4259 Nagatuta, Yokohama 226-8503, Japan

Electronic Supplementary Information (ESI) available: [details of any supplementary information available should be included here]. See DOI: 10.1039/x0xx00000x

We have investigated anion replacement and relevant material properties in mayenites, whose chemical formula can be described in analogy to Eq. (1) as:

$$[Ca_{24}Al_{28}O_{64}]^{4+}\cdot 2Y^{2-}. \qquad (2)$$

Its cubic lattice ($I\bar{4}3d$) has specific site constructed by 'cage', which is partially occupied by monovalent or divalent guest anions including (Y^{2-} =) $2F^-$, $2Cl^-$, $2OH^-$, O^{2-}, O_2^{2-}, $2O_2^-$, $2O^-$, or $2H^-$.[21] Most of these anions are the same as those for apatites, probably because of a similar environment involving local coordination with Ca^{2+} ions. In H^- ion-doped mayenite, an F^+ centre, which is a point defect of an electron localized in the free space of the cage, can be formed by UV irradiation. Inter-cage hopping of the electron induces a persistent electrical conductivity.[22] When the electron replacement becomes complete, electrons are delocalized over every cage, leading to metallic electrical conductivity.[23] The resulting crystal, in which electrons substitute certain anions, is called an electride, which was originally investigated in ionic crystals consisting of saline cation-organic molecule complexants.[24] Electrides exhibit various unique optical, chemical, electrical and magnetic properties, including low work function, which is important for electron-emission [25] and catalytic applications.[26,27]

Despite the similar structural characteristics of apatites and mayenites, formation of an H^- ion in apatites had not been reported until our recent communication.[28] In addition, neither the formation of electron centres nor electronic conductivity in calcium phosphate apatites has been achieved yet. This paper describes evidence for incorporation of H^- ions in the channel of apatite by chemical treatment under harsh reducing conditions, and photolytic formation of electrons from the H^- ions, leading to 'green apatite'.

2. Experimental

2.1 Sample preparation

Commercial calcium phosphate apatite ceramics (Cell yard™, Pentax/Asahi Techno Glass/Hoya, Japan) were used as the starting materials. The samples had diameters of 5 or 13 mm and thickness of 2 mm, nominal apatite phase fraction of >99%, and porosity of <1%. Chemical analysis by inductively coupled plasma-atomic emission spectroscopy gave a Ca/P ratio of 1.668(1), which is very close to the theoretical ratio of 10/6. The starting ceramic pellets were processed under the conditions described in Table 1. In some batches, the ceramic pellets were sliced before heat treatment. The sample denoted 'As' indicates the as-received apatite. O_2-6h and O_2-2d were annealed in dry O_2 atmosphere using a tube furnace for 6 h and 2 days, respectively. H_2O-6d was annealed for 6 h in humidified atmosphere formed by passing N_2 gas through water at a temperature of 30 °C. The H_2O partial pressure was estimated to be 0.02 atm from the saturated water vapour pressure at 30 °C. Ti-1d, Ti-2d and Ti-4d samples were annealed with metallic titanium under vacuum for 1, 2, and 4 days, respectively. In this process, slices of apatite ceramic were placed in silica glass tubes (outer diameter of 13 mm) with an excess (approximately 100 times sample weight) of Ti shot (purity of 99%, Wako, Japan), evacuated using a scroll pump and finally sealed by welding with an oxyhydrogen burner. H-1d, H-2d, H-4d, and H-20d were annealed with TiH_2 under vacuum for 1, 2, 4 and 20 days, respectively. The apatite pellets were placed with TiH_2 powder (100 mg, purity of 99%, Wako, Japan) in an envelope made of Ti foil (40-μm thick, purity of 99.5%). The envelopes were then sealed in evacuated silica glass tubes. After heat treatment, reaction layers formed on Ti- and H-series samples were removed by mechanical grinding. For optical measurements, samples were mechanically thinned to 40–200 μm in thickness and finished to a mirror surface. In some measurements, thinned samples were illuminated with UV light generated by a xenon lamp and passed through a dichromic mirror-type IR-cut filter and UV-VIS-cut filter with a 320-nm threshold with a flux of approximately 100 mW/cm^2.

Table 1 Sample annealing conditions

Name	Dimensions (mm)^a	Atmosphere / Reagent	Heat treatment (°C / days)
As	$5.0^\phi \times 2.0^t$	—	—
O_2-6h	$5.0^\phi \times 2.0^t$	1 atm O_2	1100 / 0.25
O_2-2d	$5.0^\phi \times 2.0^t$	1 atm O_2	1200 / 4
H_2O-6d	$5.0^\phi \times 0.2^t$	0.02 atm H_2O	900 / 6
Ti-1d	$8^w \times 6^l \times 1^t$	Vacuum / Ti	1000 / 1
Ti-2d	$8^w \times 6^l \times 1^t$	Vacuum / Ti	1000 / 2
Ti-4d	$8^w \times 6^l \times 1^t$	Vacuum / Ti	1000 / 4
H-1d	$8^w \times 6^l \times 1^t$	Vacuum / TiH_2	1000/ 1
H-2d	$8^w \times 6^l \times 1^t$	Vacuum / TiH_2	1000 / 2
H-4d	$8^w \times 6^l \times 1^t$	Vacuum / TiH_2	1000 / 4
H-20d	$5.0^\phi \times 2.0^t$	Vacuum / TiH_2	1000/ 20

^{a} ϕ denotes the radius of a pellet, w is the width and l the length of a slab, and t denotes thickness.

2.2 Characterization

X-ray powder diffraction (XRD) was performed using a diffractometer (Rint-2000, Rigaku, Japan) with a Cu-$K\alpha$ source principally to confirm the preservation of apatite phase and formation of minor phases after annealing.

Synchrotron XRD was carried out for selected samples (H_2O-6d, H-2d, H-4d, and O_2-2d) using a Debye-Scherrer camera with a goniometer radius of 286 mm equipped with a semiconductor detector at beam line BL15XU, SPring-8, Japan. The X-ray wavelength was 0.65273 Å, and the temperature was 300 K. High-static data with a peak intensity of ~10^6 counts was recorded with a step of ~0.003°, and analysed by Le Bail and Rietveld methods using Rietan-FP software. [29]

UV-VIS transmission spectra were measured with a spectrophotometer (U-4000, Hitachi, Japan) in a wavelength range between 200 and 3400 nm at room temperature (RT, 298 K). IR transmission spectra were measured with a spectrometer (Spectrum One, Perkin-Elmer, USA) at RT. Raman spectra were measured with a spectrometer (HR800, Horiba

Jobin Yvon, Japan) equipped with a Peltier-cooled semiconductor laser source with a wavelength of 457.4 nm. The spectrometer was controlled and collected data were processed with Labspec5 software.

X-band electron paramagnetic resonance (EPR) of the sample H-20d was performed on a spectrometer (EMX8/2.7, Bruker, Germany). Data for UV-irradiated samples were collected at RT and 77 K. The *g*-value at RT was calibrated using a solution of di(phenyl)-(2,4,6-trinitrophenyl)iminoazanium (DPPH) in benzene with a *g*-value of 2.0035. Low-temperature (1.5 K) *in situ* UV-irradiation measurements were performed with a He-flow cryostat containing a silica glass window (No. 39268.4/A, Oxford, UK) and temperature controller (ITC503, Oxford, UK). Dispersion mode was used for low-temperature measurements because severe power saturation could not be avoided in conventional absorption mode even at very small microwave power.

^{1}H magic angle spinning (MAS) nuclear magnetic resonance (NMR) spectroscopy was performed on a spectrometer (DSX-400, Bruker Biospin, Germany) operating at a resonance frequency of 400.13 MHz equipped with a high-speed MAS probe with a diameter of 4 mm. Each granulated sample (about 70 mg) was weighed to obtain a quantitative result and placed in a zirconia rotor. The rotation frequency was 15 kHz. Spectra were acquired using 45° pulses with a duration of 2.5 μs and interval of 175 s. Chloroform (+7.25 ppm with respect to tetramethylsilane, TMS) was used as a secondary reference for chemical shifts.

The concentration of H^- ions in the H-20d sample was evaluated with volumetry.[30] The weighed sample was placed in an Einhorn fermentation tube with a capacity of 5 mL. Pure water saturated with hydrogen gas was poured into the Einhorn tube and the sample powder was settled down on silica glass wool. HCl solution (37%, ~0.5 mL) was added to the water reservoir of the Einhorn tube, and then the sample started to gradually dissolve and evolve hydrogen gas. The concentration of H^- ions was calculated from volume of evolved H_2 assuming the reaction: $H^-(\text{sample}) + H^+(\text{solution}) \rightarrow H_2(g)$.

3. Results

3.1 XRD

All samples after the heat treatment were confirmed to be preserving apatite phases by XRD. Trace of CaO was found in severely reduced samples. Results of Rietveld refinement for the synchrotron XRD data were provided in ESI. In brief, H_2O-6d, H-2d, and H-4d samples were best analysed by the hexagonal $P6_3/m$ symmetry, while the symmetry of O_2-6d sample was lowered to triclinic. So far there is only one report of triclinic calcium phosphate apatite,[31] which was revealed by a high-resolution data of synchrotron XRD. Of the two possible triclinic space groups, $P\overline{1}$ was chosen for the O_2-6d sample as same as the previous study. Although the H-2d and H-4d were best analysed by the hexagonal symmetry as far as the resolution of our data, these *R*-factors were worse than that of H_2O-sample, implying the slight deformation of lattice to be lowered to the trigonal symmetry.

Table 2 summarizes the occupancy and (averaged) position of oxygen atom in channel (O4 site), which models the OH^- and O^{2-} and other oxygen-related species in the channel. Hydrogen was not considered because of its low sensitivity. Thus these occupancy and position values are expected to involve the statistic distribution of the species in the channel. Under the fully hydrated state, the occupancy is ideally 1/2 and its oxygen position is accepted to be deviated from the mirror plane at z = 1/4 and 3/4 in the hexagonal lattice (Ca_3 triangle). The fully dehydrated apatite is expected to have an occupancy of 1/4 at the position close to the mirror plane, corresponding to the presence of O^{2-} ion in the half of each Ca_3 triangle site. The estimated occupancy summarized in Table 2 suggests that the channel of H_2O sample is fully occupied by OH^- ion, while the others were evaluated to be partially dehydrated by ~30–55% so that the channel is co-occupied by OH^-, O^{2-} and possibly other species. Thus, it is convincing that the deviation of averaged oxygen position from the mirror plane became smaller as the occupancy decreases. Large thermal parameter that further increases with increasing the degree of the hydration suggests the position of OH^-, O^{2-} and other possible species are disordered.

Table 2 Rietveld refinement result of synchrotron XRD data

Sample	Occupancy of O at the channel site	Deviation of O position from the centre of Ca_3 triangle (Å)	Square root of thermal parameter (Å)
H_2O-6d	0.537(4)	0.38	1.1
H-2d	0.422(4)	0.35	1.3
H-4d	0.401(5)	0.34	1.4
O_2-2d [a]	0.41(4)	0.32	1.4

[a] Averaged values for two oxygen sites, O4a and O4b.

3.2 Optical properties

Figure 1a shows the appearances of the As and H-4d samples. Light transmittance in the apatite ceramics was especially enhanced when annealed under reducing conditions (Ti and H-series samples) for a longer duration. Thus, these processes are technically useful for obtaining translucent apatite ceramics. Optical absorption spectra obtained for As and H-4d together with a sample annealed in O_2 (O_2-2d) are presented in Fig. 1b. Because of a scattering caused by microstructural defects in the polycrystalline samples, optical transmission in the shorter wavelength range is poor in As and O_2-2d, while the transmission of H-4d is improved markedly.

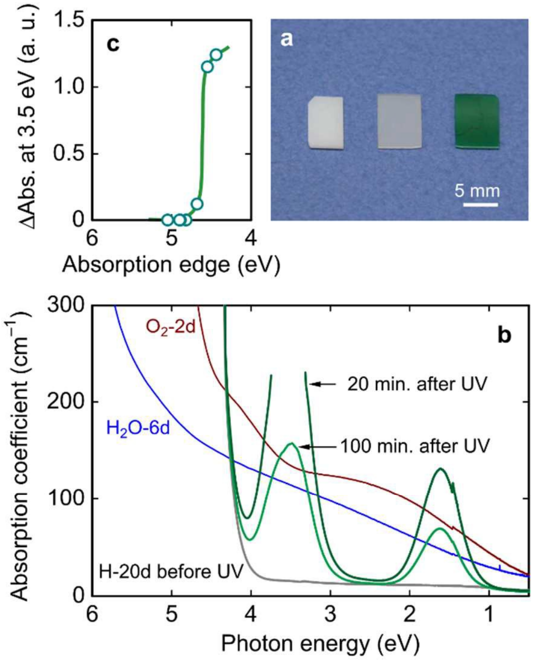

Fig. 1 Optical properties of TiH2 and Ti-processed apatite samples. (a) Appearance of as-received (left) and TiH2-processed (H-4d) samples before (centre) and after (right) illumination by UV light. (b) Absorption spectra for H2O-6d (blue), O2-2d (brown), and H-4d before (grey) and after the termination of UV-illumination for 20 minutes (deep green) and 100 minutes (light green). Reflection loss was not corrected. A spike at 1.46 eV is an artifact caused by detector switching. (c) Change in absorbance at 3.5 eV caused by UV illumination plotted against absorption-edge energy (defined by the photon energy at α = 300 cm^{-1}) in Ti and H-series samples before UV illumination.

The samples annealed in the presence of TiH_2 for a long period (H-4d and H-20d) exhibited blue-green coloration upon the illumination with UV light (Fig. 1a). Such coloration was also induced by X-ray irradiation. This coloration is caused by the emergence of two absorption bands with peaks at 3.5 and 1.6 eV, as illustrated in Fig. 1b. After ceasing UV illumination, the coloration decays at RT on the time scale of hours or days while keeping the same intensity ratio of the two bands. The kinetics of this decay will be quantitatively discussed in the next subsection. Similar coloration was also observed in Ti-series samples annealed for a long period, but was not found for As, H_2O and O_2-series samples. To quantitatively evaluate the coloration sensitivity of the H- and Ti-series samples, they were illuminated with UV light for 120 s and then the change in absorbance at 3.5 eV was measured. The measured change in absorbance is plotted against the UV absorption edge before illumination, which is defined by the photon energy at an absorption coefficient, α, of 300 cm^{-1}, in Fig. 1c. The sensitivity increases sharply when the absorption edge shifts below 4.6 eV, suggesting an absorption band around this energy range is responsible for the coloration of the samples upon irradiation with UV light.

The optical absorption of the samples below ~10^3 cm^{-1} around the absorption edge does not correspond to their intrinsic band gap; instead it contains contributions from transitions at defects and/or tail states of conduction or valence bands. According to a study on the effect of guest anions in mayenite on optical properties,[21] the absorption edge of mayenite is determined by these anions and is shifted from higher to lower energy with the order of $F^{-} > OH^{-} > O^{2-} > H^{-}$. The first three anions are common species incorporated in the channel sites of calcium phosphate apatite. According to the analogy of calcium phosphate apatite with mayenite, the absorption edge of the H_2O-6d sample, which exhibits the highest absorption edge energy of the three samples in Fig. 1b, is ascribed to OH^{-} ions in the channel sites. The next highest is observed for O_2-2d, whose major species in the channel is O^{2-} ions. The lowest-energy absorption edge, which is responsible for the photoexcited coloration, is attributed to H^{-} ions. The incorporation of H^{-} ions in the channel sites will be further substantiated by evidence described below. Because H^{-} ions can release electrons by oxidization to H^0 and H^+ states, the most feasible origin for the coloration is the formation of electron centres. Nevertheless, a change in electrical conductivity accompanying coloration was not detected in calcium phosphate apatite unlike the case of mayenite.[22] All samples irrespective of UV illumination remained insulating ($<10^{-10}$ S/cm).

3.3 EPR

Figure 2 shows EPR spectra relevant to the coloration of the calcium phosphate apatite samples. An almost isotropic signal whose intensity correlates with the absorption bands at 3.5 and 1.6 eV was observed at g = 1.9996(2) at RT. When the H-20 sample was irradiated with UV light for a few hours until saturation of coloration, the spin concentration increased up to 1×10^{19} cm^{-3}. This new signal has entirely different characteristics from those assigned to O_2^{-},[16] O^{-},[18,19,32] $^{\bullet}OH$ [20] and CO_3^{3-} [32] ions in calcium phosphate apatites. The observed signal is also not consistent with PO_3^{2-} defects, which are characterized by g-values of ~2.00 and hyperfine interactions of ~60–90 mT by ^{31}P nuclei (I = 1/2, 100% abundance).[33] The g-value is negatively shifted from that of a free electron, 2.0023. The line width was narrow (0.22 mT, signal 1 in Fig. 2a) and the signal intensity was easily saturated, for example, over ~3×10^{-5} W at RT and ~1×10^{-6} W at 77 K, suggesting a weak interaction with the lattice. These features indicate the observed signal is an electron trapped at an anion vacancy like an F^+ centre in alkaline-earth oxides.[34] The isotropic shape of the peak and weak interaction with the lattice suggest the electron is captured at the centre of a vacant Ca_6 octahedron site. The local point symmetry at the centre of the octahedron is formally trigonal, but it is very close to octahedral symmetry, leading to the isotropic g-value. The slightly displaced shape of the single Lorentzian signal is most likely caused by a hyperfine interaction with ^1H (I = 1/2, 100% abundance). The strength (A = 0.26 mT) of the interaction suggests that the electron and proton are separated by a few angstroms. The candidates for the proton include that in an OH^{-} ion at a neighbouring channel site or that in an HPO_4^{2-} group beside the channel.

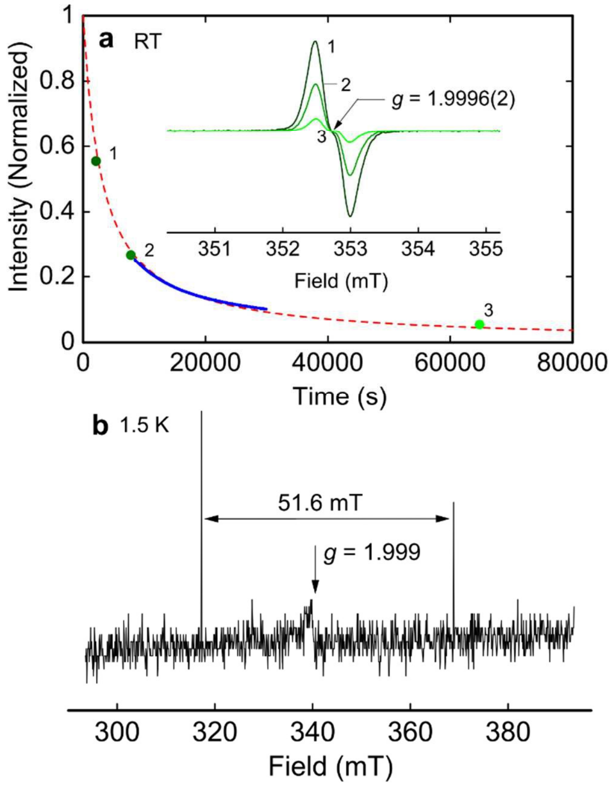

Fig. 2 EPR of a colour centre generated by UV illumination of sample H-20d. (a) Spectrum of the colour centre at RT and its decay. The three numbered spectra were measured at 2, 6, and 64 × 10^3 s after stopping UV illumination. The blue line was obtained by monitoring the intensity of the peak top at 352.3 mT. The red dashed curve is a second-order fitting curve. (b) A dispersion-mode spectrum recorded immediately (~5 s) after starting illumination with UV light at 1.5 K.

Quantitative EPR measurement revealed that the oscillator strength, *f*, of the optical absorption bands at 3.5 and 1.6 eV was 0.02 and 0.01, respectively. These intensities are typical of those of F^+ centres formed in an oxygen vacancy of alkaline-earth oxides with rock salt structure. The observed *g*-value of 1.9996(2) and absorption band at 3.5 eV are very close to those of an F^+ centre in CaO (*g*-value of 2.000 and F^+ transition energy of 3.4 eV).[34] Therefore, the 3.5-eV band can most likely be assigned to the 1s → 2p-like transition from the ground state to first excited state in an F^+ centre. In the case of CaO, however, no absorption band corresponding to the 1.6-eV band has been reported. We tentatively attribute the 1.6-eV band to charge transfer transitions to a neighbouring vacant octahedron or triangle sites that are unique to the apatite lattice and not present in CaO.

To confirm the presence of an H^- ion as the source of the F^+ centre, EPR was measured during UV irradiation at low temperature. The spectrum in Fig. 2b was obtained just after starting illumination of H-20d with UV light. The centre peak corresponds to the F^+ signal and sharp doublet separated by 51.6 mT are unambiguously assigned to a hydrogen atom (H^0). The H^0 signal quickly disappears during the measurement even at 1.5 K. The different intensities of the doublets in Fig. 2b are caused by annihilation during data collection. In contrast, the F^+ signal monotonically increased in intensity during UV illumination. These results indicate the F^+ centre is generated by photolysis of the H^- ion, and remaining H^0 can survive only a short time even at low temperature before it is converted to another nonmagnetic species. Similar behaviour has also been observed for H^- ion-doped mayenite.[35]

One pathway for the annihilation of H^0 is recombination with an electron, but this cannot account for the survival of the electron (F^+ centre) alone. The other possible pathway is release of another electron that converts H^0 to H^+, followed by a short-length diffusion of the H^+ to an oxide ion to form an OH^- ion. This reaction can leave two F^+ centres per one H^- ion. The overall reaction is described as:

$$H^- + O^{2-} \rightarrow 2e^- + OH^-. \qquad (3)$$

Such a two-electron generation reaction is supported by the decay kinetics of the F^+ centre. The decrease of the concentration of F^+ centres after UV illumination at RT (Fig. 2a) is well fitted by second-order kinetics with respect to its concentration, $[e^-]$:

$$\frac{d[e^-]}{dt} = -k[e^-]^2 , \qquad (4)$$

where *t* is time, and *k* is the rate constant, which is 3 × 10^{-22} cm^3 s^{-1} at RT. Similar decay of F^+ centres has been proposed based on experimental data collected for H^--doped mayenite using analytical equations assuming various rate-determining steps.[37] Observation of second-order kinetics supports the occurrence of the two-electron reaction given in Eq. (3). This will be discussed in greater detail in section 4.

3.4 Characterization of hydrogen

IR and Raman spectroscopy may be used to identify H^- ions in the apatite samples. If an H^- ion is incorporated in a channel site, a Ca-H stretching signal is expected to be observed in these vibrational spectra. This signal appears at around 900 cm^{-1} for H^- ions formed in CaO crystals.[38] However, the Ca-H stretching mode tends to overlap with the main vibration mode in PO_4^{3-} tetrahedron (ν_1, symmetric stretching modes) centred at 962 cm^{-1},[39,40] hindering direct observation. Thus, we used NMR spectroscopy to identify H^- in the apatite samples. To support the interpretation of NMR data, OH^- groups in different chemical environments are carefully identified.

Figure 3 displays IR transmission and Raman scattering data in the O-H stretching range collected for all of the samples. The sharp signals at 3572 cm^{-1} (band i in Fig. 3) arise from OH^- ions in the channel site.[40] The IR spectra show broad, strong bands from ~3600 to 2400 cm^{-1}. In most previous studies, these broad bands have not been identified and discussed in detail because of possible overlap with signals from adsorbed water in powder samples.[40] Here, the observed broad bands are not ascribed to absorbed water because our samples are dense ceramics. The broad bands are also not ascribed to certain electronic transitions because similar bands are also found in the Raman spectra, and one-to-one assignment to IR spectra is possible. Therefore, these signals arise from protons in the apatite lattice with stronger hydrogen bond character than that of the channel OH^- ion. These relatively strong signals are explained from the general tendency that increased strength of hydrogen bonding greatly increases the intensity of IR absorption, but not Raman scattering, because of the increased dipoles. Hereafter, semi-quantitative interpretations will be based on the IR transmission data, because the Raman measurements strongly depend on spectrometer and surface conditions. In addition, background subtraction processes markedly affect evaluation of broad signals.

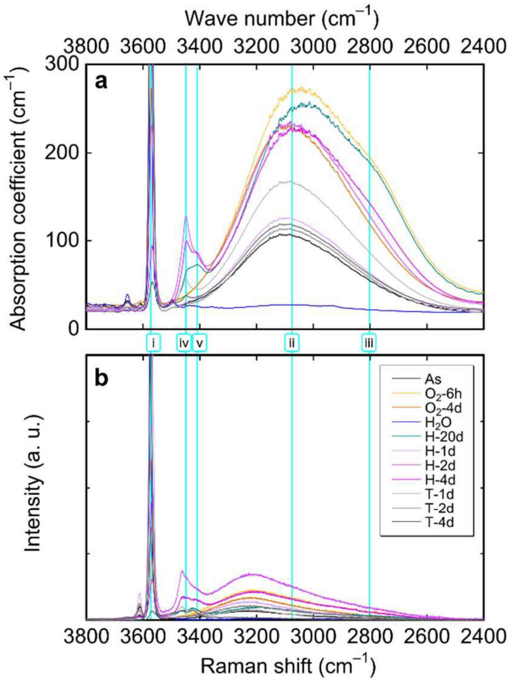

Fig. 3 (a) Infrared transmission and (b) Raman spectra of the samples in the O-H stretching range. Some data (O_2-6h, H_2O, H-20d, and H-4d in a) are replotted from Ref. 28.

The broad bands in the IR spectra can be divided into two components centred at ~3100 cm^{-1} (band ii in Fig. 3) and ~2800 cm^{-1} (band iii). Two types of hydrogen-bonded protons in apatite have been suggested, one is structural H_2O incorporated in the channel sites that forms hydrogen bonds with neighbouring PO_4^{3-} tetrahedra,[41,42] the other is acid phosphate, HPO_4^{2-}, in which the proton belongs to a PO_4^{3-} tetrahedron and forms a hydrogen bond with a neighbouring PO_4^{3-} tetrahedron.[40,42] We tentatively assign band ii to structural H_2O and band iii to HPO_4^{2-}.

Two small bands at 3408 cm^{-1} (iv) and 3448 cm^{-1} (v) are also observed for the first time in this study. These bands only appear in the spectra of chemically reduced H- and T-series samples. Detailed XRD measurements revealed that these samples contained trace CaO phase, and its content correlates with the intensity of these two bands. Freund and Wengeler [43] found that association of OH^- ions and oxygen vacancies in CaO produces various kinds of complex defects. For example, an OH^- ion/oxygen vacancy pair exhibits O-H stretching at 3417, 3429 and 3442 cm^{-1}. These values are very close those observed here, thus bands iv and v are assigned to OH^- ions in CaO precipitates in the apatite samples. In addition, the band at 3660 cm^{-1} observed for the H_2O-6d sample is most likely from $Ca(OH)_2$ [44] or complex defects consisting of two OH^- ions and an oxygen vacancy in CaO (3650 cm^{-1} [43]). The band at 3612 cm^{-1} observed in the Raman spectrum of the O2-2d sample is tentatively assigned to surface OH groups.

The absence of phosphine groups, in which P-H stretching appears in the 2320–2270 cm^{-1} range,[45] was confirmed. No pyrophosphate groups ($P_2O_7^{4-}$) with bridge stretching at 920–970 cm^{-1} [46] were detected in any of the samples.

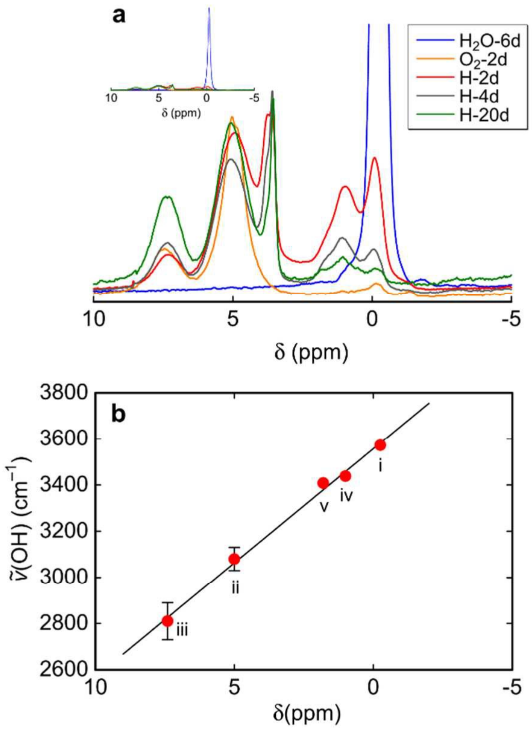

Fig. 4 ^1H MAS NMR. (a) Spectra of selected samples with respect to TMS. Data except for that of H-2d were replotted from those in Ref. 28. The inset is a full-scale plot of the same samples. (b) Correlation between O-H stretching wavenumber and ^1H chemical shift observed in a. Labels i-vii correspond to those in Fig. 3.

Figure 4a shows ^1H MAS NMR spectra of selected samples. The main peak in the H_2O sample is centred at –0.2 ppm. Its intensity markedly decreased accompanied with a slight positive shift upon TiH_2 or O_2 annealing. This signal, usually observed in the range between +0.2 ppm [41,47] and –0.2 ppm [48,49], has been assigned to structural OH^- ions.

Signals at 5.0 and 7.4 ppm tend to increase in intensity as the signal from the structural OH^- ions weakens. Although adsorbed water on fine-grained apatites often gives a broad signal around ~5 ppm [10,48], its contribution is negligible in our samples, as confirmed by the absence of this signal in the H_2O sample. These two signals are observed at lower resonant field in the spectrum of the O_2-annealed sample, and similar signals have been reported in previous studies. The intensities of the 5.0- and 7.4-ppm bands roughly correlate with those of bands (ii) and (iii) in IR spectra, respectively. Thus, they are ascribed to two types of hydrogen-bonded protons; *i.e.*, protons in structural H_2O [41,49,50] and HPO_4^{2-} groups.[9,10,47–49] The presence of the these species is supported by the occupancy of oxygen-related species in the channel evaluated by the Rietveld analysis (Table 2). The samples with well-developed 5.0 and 7.4 ppm bands has only weak signal of the structural OH^- ions. If such the nearly full dehydration is compensated by solely the formation of O^{2-} ion in the channel, the occupancy of channel should be close to 1/4. In fact, the observed occupancy was larger than the ideal value of 1/4, for example by ~60% for O_2-2d sample. The presence of structural H_2O or HPO_4^{2-} groups account for such the excess occupancy. The formation of H_2O group contribute to enhance the channel occupancy without the restriction of the electro-neutrality of channel, while the electro-neutrality for the effectively positive charge of HPO_4^{2-} group is compensated by excess O^{2-} ion or other negative species in the channel.

The NMR signals at 1.0, 1.8 and 3.4 ppm are unique to samples in this study. The intensities of the signals at 1.0 and 1.8 ppm roughly correlate with those of bands iv and v in IR spectra, respectively. Thus, they are ascribed to the OH^- defects in CaO precipitates.

Observed proton chemical shifts are plotted against the wavenumber of the relevant O-H stretching band in Fig. 3b. A correlation between ^1H chemical shift and the distance, $d_{O\text{-}H\ldots O}$, between the oxygen atom of OH^- and counter oxygen atom of the hydrogen bond has been well established, especially for oxides containing Ca^{2+} ions.[47] It is also well known that the O-H stretching frequency has a direct correlation with $d_{O\text{-}H\ldots H}$.[51] Therefore, the good correlation observed for the points in Figure 4b is explained by the combination of these two relationships. As $d_{O\text{-}H\ldots H}$ decreases, *i.e.*, the hydrogen bond becomes stronger, the proton is more attracted to the counter oxygen, and the O-H bond strength weakens, which in turn decreases the O-H stretching frequency. At the same time, the proton is drawn out of the electron cloud of the host oxygen, weakening the magnetic shielding on the ^1H nuclei, which, in turn, shifts the resonant field to the lower side. As $d_{O\text{-}H\ldots H}$ increases, the opposite effects are expected in the hydrogen bond, increasing the O-H stretching frequency and shifting the resonant field to a higher value.[28]

An unassigned NMR signal is observed at 3.4 ppm. Because no relevant O-H stretching band was found, this signal is attributed to the H^- ion in apatite.[28] This assignment is supported by the fact that this signal appears in only H-series samples that exhibit UV-induced coloration. The H^--ion concentration in the H-20d sample was evaluated by volumetry assuming that the H^- ion is only species that reduces water to generate H_2 gas. The evaluated H^- ion concentration was $2.3\pm0.2 \times 10^{20}$ cm^{-3}. However, this includes a contribution from the oxygen vacancy/hydrogen complex defects in CaO, thus feasible assignment to H^- in apatite is 1–2 $\times$ 10^{20} cm^{-3}. This value agrees reasonably with that estimated by comparing NMR signal intensities of the 3.4-ppm band observed for H-20d and that at -0.2 ppm for H_2O-6d.

4. Discussion

It is demonstrated in the present study that annealing of calcium phosphate apatite ceramics with TiH_2 is effective for doping H^- ions, and UV (or X-ray) irradiation of the H^- ion-doped apatite can generate an electron centre. The electron centre is not directly formed by reduction but requires the support of photolysis processes and does not contribute to electronic conduction. In the following sections, the environments of the H^- ions and electron in apatite are discussed as well as their photoinduced and thermal decay reactions. The absence of electronic conductivity is understood by considering geometrical differences between the crystal structures of apatite and mayenite.

4.1. Environments of H^- ions and electrons

The Ti-reduction process dopes fewer H^- ions into calcium phosphate apatite ceramics than the TiH_2 process. In this case, the hydrogen source may be the structural OH^- ions in the apatite lattice or residual H_2O in the source materials, and they are converted to H^- ions by severe reduction conditions. Other hydride sources such as CaH_2 and $LiAlH_4$ will also be effective to dope H^- ions into calcium phosphate apatite ceramics.

In mixed anion hydride crystals, H^- ions readily coordinate with alkali or alkaline-earth cations.[28,38,52,53] Thus, the channel composed of Ca^{2+} ions is the best candidate for accommodating H^- ions. We proposed that the ^1H isotropic chemical shift for H^- ions has a linear dependence on the distance between the coordinated saline cation and hydride ion, $d_{M\text{-}H}$.[28] This dependence is explained by the fact that as the site volume of an H^- ion shrinks, electron density at the nucleus is enhanced, which shifts the resonant field higher. This relationship can be approximated to

$$\delta\ (\text{ppm}) = 0.070\ d_{M\text{-}H}\ (\text{pm}) - 11.5\ (\pm 2). \qquad (5)$$

δ for H^- ions in apatite (3.4 ppm) therefore corresponds to a Ca^{2+}-H^- distance of 214±21 pm. This value is approximately the same as the distance between the centre and a Ca^{2+} ion in the Ca_3 triangle (235 pm). Thus, each H^- ion is most likely located at the centre of a Ca_3 triangle.

Photolysis of an H^- ion produces an H atom. The observed doublet attributed to the H atom is separated by 51.6 mT. The *g*-value and hyperfine splitting constant, *A*, of the H atom are calculated to be g = 1.969 and A = 51.3 mT, respectively. The latter is greater than that for a free H atom (50.7 mT) by 1.0%. Similar positive shifts have been observed for H atoms in a Ne matrix [54] and an interstitial site in a KF crystal.[55] The positive shift suggests that the H atom is in a cramped site. The shift of 1.0% corresponds to shrinkage of the atomic radius by −0.9% and an increase in the electron density of the nucleus of +2.7%. A more remarkable feature is the large negative shift of *g* (-33.3×10^{-3}) from that of a free electron. The *g*-value of the *s*-electron in an H atom, as well as that in an F^+ centre, depends on the spin-orbit coupling arising from the interaction with surrounding cations. As the strength of this interaction increases, the amount of angular momentum (*p* and *d* character) admixed into the wave function also increases, leading to a negative shift.[34,54,56] For example, large negative shifts have been observed in F^+ centres in SrO (-17.8×10^{-3}) and BaO (-66.8×10^{-3}).[34] The present results suggest that each H atom is confined in a narrow site surrounded by Ca^{2+} ions and strongly interacts with them. It is reasonable that each H^- ion confined in the centre of a Ca_3 triangle is simply photolyzed to an H atom while staying at the same site. The H atom in apatite has obviously different character from that in β-$Ca_3(PO_4)_2$, where the H atom located between two PO_4^{3-} tetrahedra is preserved even at RT.[57]

The negative Δg for the F^+ centre in apatite (-2.7×10^{-3}) is one order of magnitude less than that of an H atom. This result supports the electron occupying the centre of the Ca_6 octahedron site, where the distance between the centre and Ca^{2+} ion (291 pm) is much larger than that in the Ca_3 triangle site. The formation process and environment of the F^+ centre in apatite are analogous to that of an F_S^+(H) centre on an MgO surface. In this case, an H^- ion formed on a surface site of dehydrated MgO is photolyzed to release electrons, forming electron centre(s) on a surface anion defect site that are termed F_S^+ centres. The H^+ ion produced is stabilized on the surface of an O^{2-} anion by forming an OH^- group in close proximity to the electron centre. The F_S^+(H) centre is the complex of these species. The electron and proton distance of the F_S^+(H) centre of about 230 pm gives a hyperfine interaction of 0.27 mT, [56,58] which is almost the same intensity as that observed in our experiment (Fig. 2a). Because the distance between Ca_3 triangles is 340 pm, the nearest hydrogen is likely located a neighbouring channel site of the electron-occupied Ca_6 octahedron. The hydrogen is most likely stabilized in the form of a structural OH^- ion.

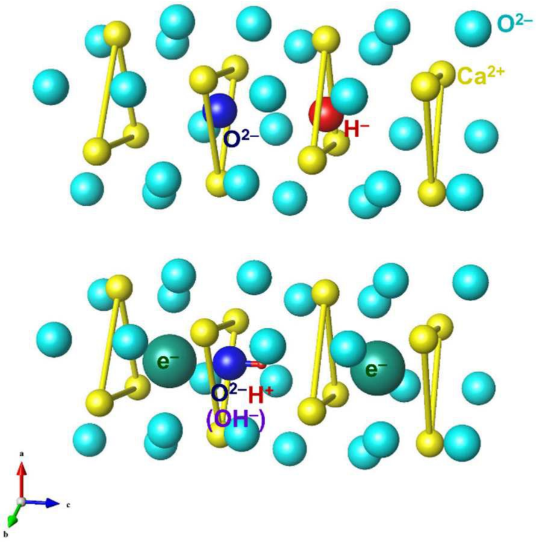

Fig. 5 Model for H^- ion and electron (F^+ centre) in the channel of calcium phosphate apatite. The upper and lower diagrams correspond to the left (as-prepared) and right (after photoillumination) sides of Eq. 3, respectively.

As summarized in Fig. 5, the two-electron process described by Eq. 3 is substantiated in this study: the photolysis of an H^- ion to create the first electron and H^0, as observed in low-temperature EPR; the second electron is thermally released and the remaining H^+ combines with an O^{2-} ion to form an OH^- ion. The kinetics of the reverse reaction of Eq. 3 have been discussed in Ref. 36 and 37. There are three elemental steps that determine the reaction order with respect to the electron concentration: i) dissociation of OH^- to release a proton; ii) coalescence of a proton and electron to form H^0; iii) further electron capture to form an H^- ion. If the elemental reaction i) is the rate-determining step, pseudo zero-order kinetics will be observed, while pseudo first-order kinetics are expected for reaction ii) and pseudo second-order kinetics for reaction iii). The experimental observation of second-order kinetics indicates that electron capture by H^0 is the rate-determining step. This interpretation further implies that the supply of protons from OH^- groups is fast compared with the electron capture reaction. This is logical because partially dehydrated hydroxyapatite is a good proton conductor [59,60]. Moreover, the absence of electrical conductivity in our samples indicates that electron mobility is quite low, limiting the chance of capture by H^0. These conditions are different from the kinetics of H^- ion-doped mayenite, where the caged OH^- ions are thermodynamically very stable [21,61] and electron concentration and mobility are high enough (~10^{19} cm^{-3} and ~0.1 $cm^2/s/V$, respectively) [23] that electron decay obeys zero-order kinetics.[37] Physical properties and spectroscopic parameters between apatite and mayenite are summarized in Table 3.

4.2. Modification of Apatites to Hydrides and Electrides, and their Electronic Conductivity

Table 3 Comparison of Apatite and Mayenite

		Apatite	Mayenite
Structural formula		$[Ca_{10}(PO_4)_6]^{2+}\cdot X^{2-}$	$[Ca_{24}Al_{28}O_{64}]^{4+}\cdot 2Y^{2-}$
Guest anion site		1D array of Ca_3 triangles	Cages connected with bcc geometry
OH^-	$d_{O\text{-}H\ldots O}$ (pm)	305 [a]	313 (Ref. 28)
	$\nu_{O\text{-}H}$ (cm^{-1})	3572	3540 (Ref. 61)
	δ (ppm)	−0.2	−0.8 (Ref. 28)
H^-	$d_{Ca\text{-}H}$ (pm)	235	240 (Ref. 28)
	δ (ppm)	3.4	5.1 (Ref. 28)
	Maximum occupancy	~0.03–0.06 [b]	1 (Ref. 28)
H^0	g	1.969	2.002 (Ref. 35)
	A (mT)	51.3	48.6 (Ref. 35)
F^+ (e^-)	g	1.9996	1.994 (Ref. 22)
	Maximum occupancy	~0.003 [b]	1 (Ref. 23)
	Conduction property	Insulator	Hopping when dilute; metallic when concentrated (Ref. 23)
Kinetics of reaction:	Reaction order	Second	Zero (Ref. 37)
$2e^- + OH^- \rightarrow H^- + O^{2-}$	Rate determining step	Electron capture by H^0	Dissociation of OH^- (Ref. 37)

[a] Estimated from the nearest oxygen from the structural OH^-.

[b] The maximum values achieved in the present study.

The observed phenomenon of apatite doped with H^- ions, photolysis of electrons (F^+ centre) *via* a two-electron reaction, is very similar to that found for mayenite. Apatite and mayenite possess many common crystallographic features. Each has an oxide lattice with an anion site for both monovalent and divalent anions with site volume larger than that of an oxide ion. The OH^- site is especially suitable for substitution of H^- in terms of ionic size, valence, and source of hydrogen. These similar crystallographic features of apatite and mayenite make them good candidates for H^--ion doping and as precursors for inorganic electrides. We propose that annealing with metal hydride to dope H^- ions and confirmation of doping by the techniques used in the present study can serve as a screening method to identify inorganic electride precursors. Unfortunately, direct chemical electron doping was not achieved in apatite as it is in mayenite. In apatite, the maximum H^- concentration achieved by the TiH_2 process at 1100 °C [23] and maximum electron concentration generated by UV illumination are only ~0.03–0.06 and ~0.003 of the theoretical maxima, respectively. It is obvious that hydride ions and electrons in apatite are thermodynamically less stable than those in mayenite.

A difference in the crystallographic features of apatite and mayenite is the connection geometry between anion sites. The anion sites are connected *via* Ca-O-Al-O-Al-O rings in the body-centred cubic geometry of mayenite, while they are formed by a one-dimensional array of Ca_3 triangles in apatite. Because occupation of the cage is at most 1/3, there must empty neighbouring cages among eight neighbours, allowing electron hopping. In our samples exhibiting photosensitive coloration, such as H-20d, the chemical composition is approximated to oxyapatite, $[Ca_{10}(PO_4)_6]^{2+}\cdot O^{2-}$, which corresponds to one of each two layers of Ca_3 triangles being occupied by an O^{2-} ion on average. Thus, neighbouring empty channel sites for an electron are usually separated by O^{2-} ions, hindering continuous electron hopping that leads to a macroscopic electrical conductivity. Nevertheless, the observation of charge transfer band at 1.6 eV suggests that only the local hopping of electrons occurs. Elimination of the O^{2-} ions will be required to observe the electronic conductivity in apatite and physical properties unique to its one-dimensional character, as in the one-dimensional channel in organic electrides.[24] Unfortunately, this study suggests that elimination of O^{2-} from pure calcium phosphate apatite is thermodynamically difficult. However, the apatite lattice allows substitution of various cations including transition metals and rare-earth cations at both Ca and P sites. Indeed, very recently an electron confinement in channel of lanthanum silicate apatite was reported.[62] Combination of these cations with H^- ions that release electrons upon photo-illumination is expected to provide a platform for designing new materials with functions in fields such as catalysis, fluorescence and phosphorescence, magnetism, and bioactivity.

5. Conclusions

Incorporation of H^- ions into apatite by a solid-state reduction technique was examined, and photolysis of the incorporated H^- ions to create electron centres in the channel sites of apatite was demonstrated. The typical H^- ion concentration was 1–2 × 10^{20} cm^{-3} after a dense apatite ceramic was annealed with TiH_2 at 1100 °C under vacuum. Irradiation of the H^--doped apatite with UV light at RT gives rise to green coloration originating from F^+ centres, which are characterized by optical absorption bands at 3.5 and 1.6 eV, and a g-value of 1.9996 at RT. H^0 atoms were detected by EPR only just after UV irradiation at 1.5 K. The maximum electron concentration of the sample was ~1 × 10^{19} cm^{-1} after UV irradiation at RT. The reactions for the UV-induced electron generation and decay can be summarized as: $H^- + O^{2-} \leftrightarrow 2e^- + OH^-$. The isotropic chemical shift of H^- in the doped apatite samples is +3.4 ppm. The H^- ions and transiently formed H^0 atoms are located at the centre of Ca_3 triangles, while the photo-generated electrons are likely located in the centre of Ca_6 octahedra. The absence of electronic conductivity in the doped apatite samples is ascribed to the fact that the O^{2-} ions in channel sites hinder electron hopping between vacant channel sites. Since diverse combinations of cations and anions form apatite crystals, their combination with the H^- ion or the electron in the channel is expected to create further novel properties.

Acknowledgements

This research was supported by an Elements Strategy Initiative Project to Form Core Research Centres, from the Ministry of Education, Culture, Sports, Science and Technology of Japan. We thank Drs. M. Tanaka, Y. Katsuya, O. Sakata, and N. Ohashi for synchrotron XRD measurement, and Dr. Y. Hashimoto and Ms. M. Nayuki for NMR measurements. The synchrotron XRD experiments were performed with the approval of the NIMS Synchrotron X-ray Station (Proposals No. 2013A4710). HH was supported by Accel Project, Japan Science and Technology Agency, Japan.

Notes and references

1 M. Pasero, A. R. Kampf, C. Ferraris, I. Pekov, J. Rakovan, T. J. White, *Eur. J. Mineral.*, 2010, **22**, 163.
2 R. Z. Legeros, *Calcium phosphates in oral biology and medicine*, in: Monographs in oral science, Vol. 15, Ed. H. Meyer, 1991.
3 M. Vallet-Regi, D. Arcos, *Biomimetic nanoceramics in climical use*, RSC Publishing, Cambridge, 2008.
4 X. Chen, J. V. Weight, J. L. Conca, L. M. Peurrung, *Environ. Sci. Technol.*, 1997, **31**, 624.
5 H. Tanaka, T. Watanabe, M. Chikazawa, *J. Chem. Soc. Faraday Trans.*, 1997, **93**, 4377.
6 K. Kaneda, T. Mizugaki, *Energy Environ. Sci.*, 2009, **2**, 655.
7 T. Kawasaki, *J. Chromatogra. A*, 1991, **544**, 147.
8 B. M. J. Smets, *Mater. Chem. Phys.*, 1987, **16**, 283.
9 R. M. Wilson, J. C. Elliott, S. E. P. Dowker, L. M. Rodriguez-Lorenzo, *Biomater.*, 2005, **26**, 1317.
10 C. Jäger, T. Welzel, W. Meyer-Zaika, M. Epple, *Magn. Reson. Chem.*, 2006, **44**, 573.
11 P. A. Henning, A. R. Landa-Cánovas, A. K. Larssona S. Lidina, *Acta Cryst.*, 1999, **B55**, 170.
12 N. H. de Leeuew, J. R. Bowe, J. A. L. Rabone, *Farad. Discuss.*, 2007, **134**, 195.
13 Y. Suetsugu, J. Tanaka, *Mater. Sci. Mater. Med.*, 2002, **13**, 767.
14 H. R. Low, C. Ritterb T. J. Whitea, *Dalton Trans.*, 2010, **39**, 6488.
15 H. Zhao, X. Li, J. Wang, S. Qu, J. Weng, X. Zhang, *J. Biomed. Mater. Res.*, 2000, **52**, 157.
16 J. Dugas, C. Rey, *J. Phys. Chem.*, 1977, **81**, 1417.
17 B. Segali, G. W. Dudwid, H. H. Woodbury, P. D. Johnson, *Phys. Rev.*, 1962, **128**, 76.
18 M. Mengeot, R. H. Bartam, O. R. Gilliam, *Phys. Rev. B*, 1975, **11**, 4110.
19 P. Mones, F. Callens, S. Van Doorslaer, P. Matthys, *Phys. Rev. B.*, 1996, **53**, 5190.
20 D. Close, M. Mengeot, O. R. Gilliam, *J. Chem. Phys.*, 1981, **74**, 5497.
21 K. Hayashi, M. Hirano, H. Hosono, *Bull. Chem. Soc. Jpn.*, 2007, **80**, 872.
22 K. Hayashi, M. Matsuishi, T. Kamiya, M. Hirano, H. Hosono, *Nature*, 2002, **419**, 462.
23 S. Kim, S. Matsuishi, T. Nomura, Y. Kubota, M. Takata, K. Hayashi, T. Kamiya, M. Hirano, H. Hosono, *Nano Lett.*, 2007, **7**, 1138.
24 J. L. Dye, *Inorg. Chem.*, 1997, **36**, 3816.
25 Y. Toda, S. Matsuishi, K. Hayashi, K. Ueda, T. Kamiya, M Hirano, H. Hosono, *Adv. Mater.*, 2004, **16**, 685.
26 M. Kitano, Y. Inoue, Y. Yamazaki, F. Hayashi, S. Kanbara, S. Matsuishi, T. Yokoyama, S.-W. Kim, M. Hara, H. Hosono, *Nat. Chem.*, 2012, **4**, 934.
27 Y. Toda, H. Hirayama, N. Kuganathan, A. Torrisi, P. V. Sushko, H. Hosono, *Nat. Commun.*, 2013, **4**, 2378.
28 K. Hayashi, P. V. Sushko, Y. Hashimoto, A. L. Shluger, H. Hosono, *Nat. Commun.*, 2014, **5**, 3515.
29 F. Izumi, K. Momma, *Solid State Phenom.*, 2007, **130**, 15.
30 T. Yoshizumi, Y. Kobayashi, H. Kageyama, K. Hayashi, *J. Phys. Chem., C* 2012, **116**, 8747.
31 P. Alberius-Henning, E. Adolfsson, J. Grins, *J. Mater. Sci.*, 2001, **36**, 663.
32 J. Sadlo, P. Matthys, G. Vanhaelewyn, F. Callens, J. Michalik, *J. Chem. Soc. Farad. Trans.*, 1998, **94**, 3275.
33 D. L. Griscom, E. J. Friebele, K. J. Long, J. W. Fleming, *J. Appl. Phys.*, 1983, **54**, 3743.
34 B. Henderson, *Anion vacancy centres in alkaline earth oxides*, CRC Critical Reviews in Solid State and Materials Science, pp. 1–58 1980.
35 S. Matsuishi, K. Hayashi, M. Hirano, H. Hosono, *J. Am. Chem. Soc.*, 2005, **127**, 12454.
36 K. Hayashi, P. V. Sushko, A. L. Shulger, M. Hirano, H. Hosono, *J. Phys. Chem. B*, 2005, **109**, 23836.
37 K. Hayashi, *J. Phys. Chem. C*, 2011, **115**, 11003.
38 R. Gonzalez, Y. Chen, M. Mostoller, *Phys. Rev. B*, 1981, **24**, 6862.
39 P. N. de Aza, F. Guitián, C. Santos, S. de Aza, R. Cuscó. L. Artús, *Chem. Mater.*, 1997, **9**, 916.
40 S. Koutsopoulos, *J. Biomed. Mater. Res.*, 2002, ***62***, 600.
41 T. Isobe, S. Nakamura, R. Nemoto, M. Senna, H. Sfihi, *J. Phys. Chem. B.*, 2002, **106**, 5169.
42 D. Zahn, O. Hochrein, *J. Solid. State. Chem.*, 2008, **181**, 1712.
43 F. Freund, H. Wengeler, *J. Phys. Chem. Solids.*, 1982, **42**, 129.
44 P. Dawson, C. D. Hadfield, G. R. Wilkinson, *J. Phys. Chem. Solids*, 1973, **34**, 1217.
45 T. C. Stringfellow, J. D. Trudeau, T. C. Farrar, *J. Phys. Chem.*, 1993, **97**, 3985.
46 A. Hezel, S. D. Ross, *Spectrochim. Acta*, 1967, **23A**, 1583.
47 J. P. Yesinowski, H. Eckert, *J. Am. Chem. Soc.*, 1987, **109**, 6274.
48 J. Arends, J. Christoffersen, M. R. Christerffersen, H. Eckert, B. O. Bowler, J. C. Heughebaert, G. H. Nancollas, J. P. Yesinowski, S. J. Zawacki, *J. Cryst. Growth*, 1987, **84**, 515.
49 P. Hartmann, C. Jäger, St. Barth, J. Vogel, K. Meyer, *J. Solid State Chem.*, 2001, **160**, 460.
50 J. E. Goldenberg, Z. Wilt, D. V. Schermerhorn, J. D. Pasteris, C. H. Yoder, *Amer. Miner.*, 2015, **100**, 274.
51 T. Steiner, *Angew. Chem. Int. Ed.*, 2002, **41**, 48.
52 D. A. Lang, J. V. Zaikina, D. D. Lovingood, T. E. Gedris, S. E. Latturner, *J. Am. Chem. Soc.*, 2010, **132**, 17523.
53 M. Boss, D. Petri, F. Pickhard, P. Zönnchen C. *Z.* Röhr, *Anorg. Allg. Chem.*, 2005, **631**, 1181.
54 S. N. Foner, E. L. Cochran, V. A. Bowers, C. K. Jen, *J. Chem. Phys.*, 1960, **32**, 963.
55 J. M. Spaeth, M. Sturm, *Phys. Stat. Sol.*, 1970, **42**, 739.

56 D. M. Murphy, R. D. Farley, I. J. Purnell, C. C. Rowlands, A. R. Yacob, M. Cristina Paganini, E. Giamello, *J. Phys. Chem., B* 1999, **103**, 1944.
57 K. Nakashima, J. Yamauchi, *J. Am. Chem. Soc.*, 2005, **127**, 1606.
58 M. Chiesa, M. Cristina Paganini, E. Giamello, D. M. Murphy, C. Di Valentin, G. Pacchioni, *Acc. Chem. Res.*, 2006, **39**, 861.
59 K. Yamashita, K. Kitagaki, T. Umegaki, *J. Am. Ceram. Soc.*, 1995, **78**, 1191.
60 M. Yashima, Y. Yonehara, H. Fujimori, *J. Phys. Chem. C.*, 2011, **115**, 25077.
61 K. Hayashi, M. Hirano, H. Hosono, *J. Phys. Chem. B.*, 2005, **109**, 11900.
62 Y. Zhang, Z. Xiao, T. Kamiya, H. Hosono, *Phys. Chem. Lett.*, 2015, **6**, 4966.